

## Post-Print of the Solid-State Reaction Between Mn-Si Deoxidation Alloy and MnO-SiO<sub>2</sub>-FeO Oxide During 1473K Heat Treatment

**Authors:** Liu Chengsong, Li Jingshe, Gao Xiangzhou, Yang Shufeng

**Date:** 2016-11-05T00:00:00+00:00

### Abstract

Using the diffusion couple method, the solid-state reaction between Mn-Si deoxidation alloy and MnO-SiO<sub>2</sub>-FeO oxide during heat treatment at 1473 K and its influence on the composition and phase of both were investigated using a high-temperature confocal laser microscope and a high-temperature induction furnace. The changes in equilibrium composition between alloy and oxide during solidification and the high-temperature solid-state reaction mechanism were also discussed and analyzed. The results show that the solid-state reaction occurring between alloy and oxide during heat treatment caused loss of Mn and Si elements in the alloy, a large number of MnO-SiO<sub>2</sub> particles formed in the alloy near the interface, elemental Fe particles were produced in the oxide due to decomposition of the FeO component, and the contents of MnO and FeO showed increasing and decreasing trends respectively with increasing heat treatment time.

### Full Text

### Preamble

ACTA METALLURGICA SINICA

### Solid-State Reaction Between Mn-Si Deoxidized Alloy and MnO-SiO<sub>2</sub>-FeO Oxide During Heat Treatment at 1473 K

**LIU Chengsong, YANG Shufeng, LI Jingshe, GAO Xiangzhou**

School of Metallurgical and Ecological Engineering, University of Science and Technology Beijing, Beijing 100083

### Abstract

In order to control the physicochemical characteristics of inclusions in steel through appropriate heat treatment processes, the solid-state reaction between Mn-Si deoxidized solid alloy and MnO-SiO<sub>2</sub>-FeO oxide was investigated using a diffusion couple method with a high-temperature confocal scanning laser microscope (CSLM) and induction furnace. The reaction between Fe-Mn-Si alloy and MnO-SiO<sub>2</sub>-FeO oxide during heat treatment at 1473 K and its influence on the compositions and phases of both materials were examined, along with analysis of equilibrium composition changes during solidification and the high-temperature solid-state reaction mechanism. A suitable method for pre-melting the oxide and preparing the diffusion couple was developed to ensure good contact between the Fe-Mn-Si alloy and MnO-SiO<sub>2</sub>-FeO oxide. The diffusion couple sample, together with Ti foil to reduce oxygen partial pressure and a bulk alloy of identical composition, was sealed in a quartz tube for subsequent heat treatment experiments. Quantitative elemental analysis of the alloy and oxide was calibrated using standard samples before analysis. The results demonstrated that solid-state reaction and elemental diffusion occurred between the Fe-Mn-Si alloy and MnO-SiO<sub>2</sub>-FeO oxide, indicating that the alloy and oxide in the diffusion couple were not equilibrated at 1473 K, even though their liquid phases were equilibrated at 1873 K. The activity of FeO in the MnO-SiO<sub>2</sub>-FeO oxide decreased with decreasing temperature, causing excess oxygen to diffuse from the oxide to the alloy. Mn and Si contents in the alloy were consumed by chemical reactions, generating numerous MnO-SiO<sub>2</sub> particles near the interface, while decomposition of FeO in the oxide produced elemental Fe particles. As heat treatment time increased from 10 to 50 h, the widths of the particle precipitation zone (PPZ) and manganese depleted zone (MDZ) increased from 79 and 120 μm to 138 and 180 μm, respectively, with the MDZ width always exceeding that of the PPZ. Moreover, due to FeO separation, pure Fe particles formed in the oxide, and the MnO and FeO contents in the oxide showed increasing and decreasing trends, respectively, with prolonged heat treatment time.

**Keywords:** inclusions, diffusion couple, solid-state reaction, heat treatment

---

## Introduction

Non-metallic inclusions in steel primarily consist of deoxidation products in the molten steel. Certain inclusions with high melting points and hardness can severely degrade the toughness, fatigue properties, and ductility of the steel matrix. In steel production, composite deoxidizers such as Si-Mn, Si-Ca, and Si-Mn-Al are widely used to obtain mixed deoxidation products with lower melting points that readily agglomerate into large particles, thereby accelerating their flotation and removal. Therefore, determining the types of deoxidation products in equilibrium with specific steel compositions to avoid formation of high-melting-point inclusions such as Al<sub>2</sub>O<sub>3</sub>, CaO · 2Al<sub>2</sub>O<sub>3</sub>, and SiO<sub>2</sub> is crucial for improving steel quality. However, the final non-metallic inclusions formed in the steel matrix after heat treatment and rolling processes often differ significantly

from the initial inclusions present before solidification. One major reason is that subsequent heat treatment not only alters the microstructure and properties of metallic materials but also affects internal non-metallic inclusions. Solid-state reactions can occur between the metallic matrix and inclusions, causing steel matrix segregation, modification of existing inclusions, and precipitation of new inclusions.

Previous studies have investigated these phenomena. Shibata et al. employed diffusion couples to study solid-state reactions between Fe-Cr alloy and MnO-SiO<sub>2</sub> oxide at 1473 K, finding that MnO-SiO<sub>2</sub> inclusions could transform into MnO-Cr<sub>2</sub>O<sub>3</sub> inclusions when Si content was low, but remained stable at higher Si contents. Choi et al. examined inclusion evolution in Al-Ti deoxidized alloys at 1473 K, observing that original inclusions such as pure Al<sub>2</sub>O<sub>3</sub>, Al-Ti-O, and TiO transformed into Al-Ti-Fe-O, Al-Fe-O, and Fe-Ti-O types during heat treatment. Ohba et al. investigated the formation mechanism of oxide inclusion particles in internal oxide layers at steel surface cracks, reporting that after sufficient heat treatment time, inclusion particle sizes stabilized at approximately 0.2 μm and 0.3 μm at 1473 K and 1573 K, respectively. The inclusions consisted mainly of MnO-SiO<sub>2</sub> and MnO-Cr<sub>2</sub>O<sub>3</sub> types, with a formation mechanism involving initial precipitation of MnO-SiO<sub>2</sub> particles in the internal oxide layer, followed by formation of MnO-Cr<sub>2</sub>O<sub>3</sub> on these particles, where the precipitation amounts of both phases determined the final inclusion size. These studies demonstrate that controlling the physicochemical characteristics of non-metallic inclusions through appropriate heat treatment is feasible.

Typically, electron probe microanalyzer (EPMA) or scanning electron microscopy with energy-dispersive X-ray spectroscopy (SEM-EDS) are used to directly observe and analyze changes in inclusion morphology and composition after heat treatment. However, due to the extremely small size of non-metallic inclusions, changes resulting from solid-state reactions with the alloy matrix are often difficult to detect. Moreover, most research has focused on changes in inclusion characteristics themselves during heat treatment, with limited investigation of the interface region between inclusions and the alloy matrix and its influence on alloy composition and properties. This study utilizes high-temperature confocal scanning laser microscopy (CSLM) and an induction furnace with diffusion couples to investigate the solid-state reaction between Mn-Si deoxidized alloy and MnO-SiO<sub>2</sub>-FeO oxide after heat treatment at 1473 K, its effects on the composition and phases of both materials, and the changes in equilibrium composition during solidification and the high-temperature solid-state reaction mechanism.

## Experimental Methods

The Fe-Mn-Si alloy matrix and MnO-SiO<sub>2</sub>-FeO oxide used in the diffusion couple experiments were based on high-temperature equilibrium compositions at 1873 K. The alloy composition (mass fraction, %) was: Fe 96.7, Mn 3.20, Si 0.10, S < 0.009. The oxide contained 66% MnO, 31% SiO<sub>2</sub>, and 3% FeO. To achieve

good adhesion between the solid alloy matrix and oxide, the oxide was pre-melted using a VL2000DX-SVF17SP CSLM. The alloy was cut into regular blocks, and semicircular holes approximately 1.5 mm in diameter were drilled on the alloy surface to hold oxide powder ground to less than 147  $\mu\text{m}$ . Both were placed in a CSLM crucible (inner diameter 4.5 mm, outer diameter 5 mm, height 5 mm). [Figure 1: see original paper] shows the longitudinal cross-section of the pre-melting experimental setup. The initial vacuum was  $<5.0 \times 10^{-3}$  Pa, and Ar gas protection was used at a flow rate of 50 mm<sup>3</sup>/min. Ti foil was wrapped around the crucible to further reduce the oxygen partial pressure. Samples were heated from room temperature to 50 K above the oxide melting point (approximately 1400 K) and then rapidly cooled. Heating and cooling rates were set at 100 and 1000 K/min, respectively.

After pre-melting, the well-bonded oxide-alloy sample, along with Ti foil for oxygen partial pressure reduction and a bulk alloy of identical composition to prevent contact with the Ti foil, was sealed in a quartz tube (outer diameter 12 mm, inner diameter 10 mm) as shown in [Figure 2: see original paper]. The tube was evacuated to  $<1.0 \times 10^{-2}$  Pa and backfilled with Ar gas at approximately  $2 \times 10^4$  Pa. The sealed quartz tube was heat-treated in a high-temperature tube furnace according to a specific temperature profile, then quenched in ice water. The bonded oxide-alloy sample was subsequently ground and polished, and the cross-section was analyzed using a JEOL JXA-8100 EPMA to examine composition, phases, and interface morphology. In this study, the heat treatment temperature was 1473 K with durations of 10 and 50 h. The overall heat treatment profile and sample designations are shown in [Figure 3: see original paper]. Sample H-0 represents the as-pre-melted condition, H-10 after 10 h at 1473 K, and H-50 after 50 h at 1473 K.

After quenching the sealed quartz tube, the heat-treated diffusion couple was removed and the longitudinal section was ground with SiC paper and polished with 0.3  $\mu\text{m}$  Al<sub>2</sub>O<sub>3</sub> paste. The analysis positions on the sample longitudinal section are shown in [Figure 4: see original paper]. When analyzing alloy composition, care was taken to avoid interference from oxide particles within the alloy and at the interface. Standard samples were used to calibrate each element in the alloy for accurate results. For analyzing oxide particle composition at the interface, the following calibration formula was applied:

$$M_{\text{oxide}} = M_{\text{analysis}} - \text{Fe}_{\text{analysis}} \times (M_{\text{steel}}/\text{Fe}_{\text{steel}})$$

where  $M_{\text{oxide}}$  and  $M_{\text{analysis}}$  are the actual and analyzed mass fractions of element M in the oxide particle, respectively;  $\text{Fe}_{\text{analysis}}$  is the analyzed Fe mass fraction in the analysis region; and  $\text{Fe}_{\text{steel}}$  and  $M_{\text{steel}}$  are the Fe and M mass fractions in the alloy, respectively. This formula assumes all Fe in the analysis region originates from the alloy, while Mn and Si from the alloy are calculated based on Mn/Fe and Si/Fe mass ratios. The difference between calculated and analyzed values represents the oxide composition.

When converting EPMA-measured elemental contents of oxides and precipitated

particles to compound compositions, the following method was used: Mn preferentially combined with S to form MnS based on measured S content; remaining Si, Fe, and Mn were directly converted to SiO<sub>2</sub>, FeO, and MnO, respectively.

## Results

### 2.1 Alloy-Oxide Interface Morphology

[Figure 5: see original paper]–[Figure 7: see original paper] show the interface morphology between the alloy and oxide after pre-melting, and after heat treatment at 1473 K for 10 and 50 h, respectively. [Figure 5: see original paper] reveals good bonding after pre-melting, with a small amount of particulate matter precipitated in the alloy near the interface. The oxide consisted mainly of gray phases, black phases, and white particles. EPMA analysis (Table 1) indicated that precipitated particles in the alloy were primarily MnO and SiO<sub>2</sub>, while the gray and black phases in the oxide approximated 2MnO · SiO<sub>2</sub> and MnO · SiO<sub>2</sub>, respectively. The white particles at position 8 were Fe particles with an average composition (mass fraction, %) of: Fe 95.7, Mn 3.9, Si 0.3, S 0.13. The region near the interface where oxide particles precipitated in the alloy is defined as the particle precipitation zone (PPZ). [Figure 6: see original paper] and [Figure 7: see original paper] show that with increasing heat treatment time at 1473 K, the PPZ width and precipitated particle size increased. The oxide continued to contain both 2MnO · SiO<sub>2</sub> and MnO · SiO<sub>2</sub> phases, while Fe particles also grew larger. Additionally, oxide composition data (Table 2 and Table 3) show that SiO<sub>2</sub> content remained essentially constant during heat treatment, while MnO and FeO contents exhibited increasing and decreasing trends, respectively.

### 2.2 Composition Changes in Alloy Near Interface

[Figure 8: see original paper] shows the Mn and Si content variations in the alloy near the interface after pre-melting and after heat treatment at 1473 K for 10 and 50 h. After pre-melting, the high-temperature interaction time was very short and cooling was rapid, causing only slight decreases in Mn and Si contents within approximately 15 μm of the interface, from initial values of 3.2% and 0.1% to minimum values of 1.8% and 0.03% (mass fraction), respectively.

After 10 h of heat treatment, Mn and Si contents were lower than initial values within about 120 μm of the interface. In the region 20–120 μm from the interface, Mn and Si contents decreased progressively closer to the interface, reaching minimum values of 1.2% and 0.001%, respectively. However, within 0–20 μm of the interface, Mn and Si contents increased slightly from these minima to approximately 1.6% and 0.06%, respectively. The region where Mn content decreased is defined as the manganese depleted zone (MDZ). Analysis revealed MDZ widths of 10 μm and 120 μm after pre-melting and 10 h heat treatment, respectively.

After 50 h at 1473 K, similar Mn and Si content variations were observed. The MDZ width increased to 180 μm, and the minimum Mn content rose slightly

to 1.5% at a location about 30  $\mu\text{m}$  from the interface. Therefore, in the region 30–180  $\mu\text{m}$  from the interface, Mn content decreased progressively closer to the interface, while within 0–30  $\mu\text{m}$ , Mn content increased from the minimum to approximately 2.2%. For Si, content decreased within about 180  $\mu\text{m}$  of the interface. In the region 50–180  $\mu\text{m}$  from the interface, Si content decreased progressively closer to the interface, reaching a minimum of 0%. Within 0–50  $\mu\text{m}$ , Si content gradually recovered from this minimum, reaching approximately 0.12% at the interface.

[Figure 9: see original paper] shows the widths of the PPZ and MDZ near the alloy-oxide interface after pre-melting and after heat treatment at 1473 K for 10 and 50 h. The MDZ and PPZ widths exhibited an approximately linear relationship, with MDZ width always exceeding PPZ width. For example, after 10 h, PPZ width was 79  $\mu\text{m}$  and MDZ width was 120  $\mu\text{m}$ ; after 50 h, PPZ width was 138  $\mu\text{m}$  and MDZ width was 180  $\mu\text{m}$ .

### 2.3 Composition and Size Distribution of Precipitated Particles in Alloy Near Interface

[Figure 10: see original paper] shows the composition and size distribution of precipitated particles in the alloy near the interface before and after heat treatment. [Figure 10a: see original paper] indicates that before heat treatment and after 10 h, precipitated particle compositions fell between pure MnO and  $2\text{MnO} \cdot \text{SiO}_2$ , essentially containing no MnS. After 50 h, most particles approximated  $2\text{MnO} \cdot \text{SiO}_2$  composition and contained 0–7% MnS. [Figure 10b: see original paper] shows that with increasing heat treatment time, the PPZ area increased from 850  $\mu\text{m}^2$  after pre-melting to 3950  $\mu\text{m}^2$  after 10 h and 6900  $\mu\text{m}^2$  after 50 h. Conversely, the number of particles smaller than 0.5  $\mu\text{m}$  decreased progressively from 81 per 1000  $\mu\text{m}^2$  after pre-melting to 39 per 1000  $\mu\text{m}^2$  after 10 h and 15 per 1000  $\mu\text{m}^2$  after 50 h. The number of particles sized 0.5–1.0  $\mu\text{m}$  also decreased with heat treatment, with little difference between the 10 h and 50 h conditions. Additionally, a small number of larger particles in the 2.0–2.5  $\mu\text{m}$  and  $>2.5$   $\mu\text{m}$  ranges were present after 10 and 50 h of heat treatment.

## Discussion

### 3.1 Equilibrium Composition Changes During Solidification

FactSage 6.3 software was used to calculate and analyze the equilibrium relationship and composition between Fe-Mn-Si alloy and MnO-SiO<sub>2</sub>-FeO oxide from 1473 to 1873 K. The composition and phase changes in the Fe-Mn-Si alloy and MnO-SiO<sub>2</sub>-FeO oxide during solidification are shown in [Figure 11: see original paper]. As shown in [Figure 11a: see original paper], Mn and Si contents in the alloy decreased with decreasing temperature from 1873 K to 1710 K. Below 1710 K, Mn content continued to decrease while Si content increased slightly. [Figure 11b: see original paper] shows that the oxide was liquid between 1600–1873 K. As temperature decreased, the liquid phase amount gradually decreased,

and solid  $2\text{MnO} \cdot \text{SiO}_2$  containing some FeO precipitated. At 1523 K, the liquid  $\text{MnO-SiO}_2\text{-FeO}$  oxide disappeared, solid  $2\text{MnO} \cdot \text{SiO}_2$  continued to precipitate, and a small amount of  $\text{MnO} \cdot \text{SiO}_2$  containing some FeO formed.

### 3.2 Solid-State Reaction Mechanism Between Alloy and Oxide

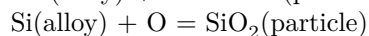
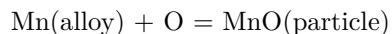
In this study, numerous inclusion particles formed at the interface between Fe-Mn-Si alloy and  $\text{MnO-SiO}_2\text{-FeO}$  oxide after heat treatment, with Mn and Si depletion and diffusion zones present in the alloy. These phenomena indicate that although the Fe-Mn-Si alloy and  $\text{MnO-SiO}_2\text{-FeO}$  oxide were in thermodynamic equilibrium at 1873 K, they became non-equilibrated and underwent solid-state reactions when temperature decreased to 1473 K.

Based on the Wagner model for activity coefficients in multicomponent solutions, the regular solution model, and relevant thermodynamic data, thermodynamic calculations were performed for  $\text{MnO-SiO}_2\text{-FeO}$  oxide compositions in equilibrium with Fe-Mn-Si alloy (containing trace  $\text{S} < 0.009\%$ ) at 1873 K and specific oxygen partial pressures. The equilibrium oxygen activity in the Fe-Mn-Si alloy at 1873 K was 0.0065, while the equilibrium FeO activity in  $\text{MnO-SiO}_2\text{-FeO}$  oxide was 0.033. Due to limited fundamental thermodynamic data for such solid-state reactions, the 1873 K thermodynamic data were extrapolated to lower temperatures for calculation. The calculated equilibrium oxygen activities in the alloy and FeO activities in the oxide at 1673 and 1473 K, and their temperature dependence, are shown in Table 4 and [Figure 12: see original paper].

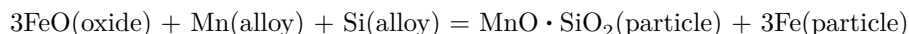
As shown in Table 4 and [Figure 12: see original paper], as temperature decreased from 1873 K to 1673 and 1473 K, the oxygen activity in the alloy decreased from 0.0065 to 0.0018 and 0.0004, respectively, while FeO activity in the oxide decreased from 0.033 to 0.022 and 0.013, respectively. The decreased oxygen activity in the alloy led to formation of a small number of inclusion particles within the alloy matrix during 1473 K heat treatment, with compositions shown in [Figure 10: see original paper]. In the oxide, the decreased FeO activity with temperature reduction caused FeO decomposition:



This reaction produced elemental Fe particles in the oxide as shown in [Figure 5: see original paper]-[Figure 7: see original paper]. Excess oxygen diffused from the oxide to the alloy interface during heat treatment, reacting with Mn and Si in the alloy to form inclusion particles at the interface:



The overall reaction can be expressed as:



Thus, particle formation at the alloy-oxide interface during 1473 K heat treatment was related to diffusion of excess oxygen from the oxide, which directly

caused the observed decreases in Mn and Si contents near the interface shown in [Figure 8: see original paper]. [Figure 13: see original paper] schematically illustrates the formation mechanism of inclusion particles at the interface.

## Conclusions

1. The deoxidation product in equilibrium with Mn-Si deoxidized alloy at 1873 K is ternary MnO-SiO<sub>2</sub>-FeO oxide. When this equilibrium system is heat-treated at 1473 K, the alloy and oxide become non-equilibrated and undergo high-temperature solid-state reactions and mutual diffusion.
2. During 1473 K heat treatment, decreased FeO activity in the oxide causes FeO decomposition, generating excess oxygen that diffuses to the alloy interface and reacts with Mn and Si in the alloy near the interface. This reaction reduces Mn and Si contents and forms MnO-SiO<sub>2</sub> particles within the alloy, while elemental Fe particles form in the oxide.
3. With increasing heat treatment time, the sizes of MnO-SiO<sub>2</sub> particles in the alloy near the interface and elemental Fe particles in the oxide gradually increase. The widths of the particle precipitation zone (PPZ) and manganese depleted zone (MDZ) also increase, while SiO<sub>2</sub> content in the oxide remains essentially constant. The MnO and FeO contents in the oxide show increasing and decreasing trends, respectively, due to the solid-state reaction.

## References

- [1] Ono H, Nakajima K, Ibata T, Usui T. *ISIJ Int*, 2010; 50: 1955
- [2] Ohta H, Suito Hideaki. *Metall Trans*, 1997; 28B: 1131
- [3] Lei H, He J C. *Acta Metall Sin*, 2004; 40: 623
- [4] Zhang B W, Deng K, Lei Z S, Ren Z M. *Acta Metall Sin*, 2007; 43: 1195
- [5] Fujii K, Nagasaka T, Hino M. *ISIJ Int*, 2000; 40: 1059
- [6] Ono H, Ibata T. *ISIJ Int*, 2011; 51: 2012
- [7] Wang X H, Li X G, Li Q, Huang F X, Li H B, Yang J. *Acta Metall Sin*, 2013; 49: 553
- [8] Jerzak W, Kalicka Z. *Arch Metall Mater*, 2012; 57: 449
- [9] Park J H, Kim D S. *Metall Trans*, 2005; 36B: 495
- [10] Lee C, Nambu S, Inoue J, Koseki T. *ISIJ Int*, 2011; 51: 2036
- [11] Takahashi I, Sakae T, Yoshida T. *Tetsu-to-Hagané*, 1967; 53: 350
- [12] Takahashi I, Sakae T, Yoshida T. *Tetsu-to-Hagané*, 1967; 53: S273
- [13] Takano K, Nakao R, Fukumoto S, Tsuchiyama T, Takaki S. *Tetsu-to-Hagané*, 2003; 89: 616
- [14] Kim H S, Lee H G, Oh K S. *Metall Trans*, 2001; 32A: 1519
- [15] Wakoh M, Sawai T, Mizoguchi S. *ISIJ Int*, 1996; 36: 1014
- [16] Wakoh M, Sawai T, Mizoguchi S. *Tetsu-to-Hagané*, 1992; 78: 1697
- [17] Shibata H, Tanaka T, Kimura K, Kitamura S. *Ironmak Steelmak*, 2010; 37: 522

- [18] Shibata H, Kimura K, Tanaka T, Kitamura S. ISIJ Int, 2011; 51: 1944
- [19] Choi W, Matsuura H, Tsukihashi F. ISIJ Int, 2011; 51: 1951
- [20] Ohba Y, Yamashita Y, Ohno K, Maeda T, Nishioka K, Shimizu M. Tetsu-to-Hagané, 2009; 95: 531
- [21] Hino M, Ito K. Thermodynamic Data for Steelmaking. Sendai: Tohoku University Press, 2010: 167
- [22] Ban-ya S. ISIJ Int, 1993; 33: 2
- [23] The Japan Institute of Metals. Physical Chemistry of Metals. Tokyo: Maruzen Press, 1996: 198
- [24] Turkdogan E T. Physical Chemistry of High Temperature Technology. New York: Academic Press, 1980: 81
- [25] Zhang J. Computational Thermodynamics of Metallurgical Melts and Solutions. Beijing: Metallurgical Industry Press, 2007: 254

*Note: Figure translations are in progress. See original paper for figures.*

*Source: ChinaXiv – Machine translation. Verify with original.*